

Analytic derivation of percolation thresholds in anisotropic systems of permeable objects

A. Drory, I. Balberg, and U. Alon

Racah Institute of Physics, Hebrew University, Jerusalem 91904, Israel

B. Berkowitz

Hydrological Service, Water Commission, Ministry of Agriculture, P.O. Box 6381, Jerusalem 91063, Israel

(Received 15 October 1990)

We present a systematic derivation of the percolation thresholds in anisotropic systems composed of permeable elongated boxes. The analytic calculation is based on an order-by-order diagrammatic expansion of the pair-connectedness function. A comparison of the results with those of Monte Carlo simulations shows excellent quantitative agreement. We conclude that, of the analytic methods suggested thus far, the present approach is the most suitable one for quantitative derivation of system properties in continuum percolation.

I. INTRODUCTION

While continuum systems are the natural and artificial systems for which percolation phenomena are of wide interest, the important advancements in the theory of percolation theory have been based on lattice models.¹ Significant results obtained for continuum percolation² were either derived from computer simulations or from extensions of lattice models. During the last decade, attempts were made to develop an independent and rigorous theory for continuum percolation, so that account can be taken of its special features. These features are the result of the variety of objects' shapes and their arrangements (e.g., angular distributions) in continuum systems. All of these attempts were based on Coniglio's relation³ between the direct pair-connectedness function $c^+(\mathbf{r})$ (related to the pair-correlation function used in the classical theory of fluids⁴) and the mean cluster size, which is a fundamental concept of percolation theory. Combined with a Percus-Yevick approximation this approach has yielded qualitative agreement with Monte Carlo simulations for systems of spheres with and without simple (hard-core) interactions.⁵ On the other hand, an alternative procedure,⁶ i.e., using Coniglio's relation with an order-by-order determination of $c^+(\mathbf{r})$, has been recently shown⁷ to yield accurate quantitative results for the percolation thresholds in systems of permeable spheres and hypercubes. In the latter derivation, advantage was taken of the availability of the well-known virial coefficients⁴ and Padé approximants (commonly used in the theory of critical phenomena⁸) to yield an excellent agreement between theory and experiment.

The next theoretical challenge is to adopt Coniglio's theory for analytic determination of percolation thresholds in macroscopically anisotropic systems made of "anisotropic" (e.g., elongated) objects. In particular, systems made of permeable anisotropic objects exist in two important areas of applications: porous media⁹ and conduction processes in disordered semiconductors.¹⁰ Relevant theoretical attempts^{11,12} have been confined so far to

Percus-Yevick-like approaches and these were applied only to systems which are *macroscopically isotropic*. Again, as for spherical objects, these approaches have yielded poor quantitative agreement with Monte Carlo results and were limited to certain ranges of object "anisotropy" (aspect ratio). A discussion of these attempts (and comparison with the method to be applied here) will be given in the final section of this paper.

In view of the above considerations we have adopted the order-by-order procedure^{6,7} for the calculation of percolation thresholds as a function of the macroscopic anisotropy in systems which consist of anisotropic objects. For such objects we do not have virial integrals^{4,13} and the corresponding object overlap integrals had to be determined for the first time. For the sake of simplicity of the calculation, and the transparency of the method, we have chosen for the calculation a system of objects which enables an analytic determination of these integrals: elongated boxes aligned along the three principal Cartesian axes. Hence, while the integrals are by no means trivial, they involve only simple one-dimensional integrations. We expect that this system of boxes captures the essential features of all systems made of elongated objects. Such expectation is borne out by the possible existence of a general definition of the macroscopic anisotropy^{14,15} and the fact that in the limit of high object anisotropy (large aspect ratio) the macroscopically isotropic system of a random distribution of object orientations has the same percolation threshold as a system where the objects are equally distributed along the principal Cartesian axes.¹⁴ To check the quantitative adequacy of the analytic results obtained we have performed, in parallel, Monte Carlo simulations. The simulations were carried out in a manner previously described¹⁵ but an efficient algorithm¹⁶ which divides the continuum into subcubes (for the determination of intersecting objects) was used. The clustering was then carried out by our continuum version¹⁶ of the Hoshen-Kopelman algorithm.¹⁷ The results to be given here were computed by averages over five samples. The sizes of our samples were such that they

had a critical concentration N_c which was between 20 000 and 40 000 objects.

II. CALCULATION OF THE EXPANSION COEFFICIENTS

Before turning to the actual description of the calculation method, we recall that Coniglio and co-workers³ have shown that the average cluster size S is given in terms of the direct pair-connectedness function $c^+(\mathbf{r})$, i.e.,

$$S = 1/[1 - \rho c^+(0)] , \tag{1}$$

where $c^+(0) = \int c^+(\mathbf{r}) d\mathbf{r}$ and ρ is the density of objects in the system. Thus the percolation onset occurs at the critical object density $\rho_c = 1/[c^+(0)]$. Since the diagrammatic expansion of $c^+(0)$ is well documented^{6,7} we emphasize here only the novel features of the present expansion which correspond to a much more general case.

Turning to these features we note that not only the statistical weights but also the integrals corresponding to the various possibilities of overlap between anisotropic permeable objects have not been calculated before. We investigate then a system of elongated boxes which are aligned along the three perpendicular directions in space, denoted here as 1,2,3. A type-1 box refers to a box whose long edge is placed parallel to axis 1, and so on. In order to simplify somewhat the calculations, we have chosen boxes with two equal edges, of length d , and an ‘‘anisotropic’’ (or ‘‘elongated’’) edge L ($L \geq d$).

We have calculated here only the first three orders in $c^+(0)$, denoted^{6,7} c_2^+ , c_3^+ , and c_4^+ . We note, however, that for the direct substitution in the formula for S [Eq. (1)] to provide good quantitative results, three terms are not enough. On the other hand, higher orders are much more complicated and require tedious calculations. One then naturally follows a common procedure⁸ for the evaluation of the contribution of high orders by using biased Padé approximants.⁷ Indeed as we show below this is sufficient to get an excellent quantitative agreement with the experimental data.

In the order-by-order expansion^{6,7} of the usual ‘‘isotropic objects’’ case we have that

$$c_2^+ = \text{O} \cdots \text{O} = \int f^+(\mathbf{r}) d^3r , \tag{2}$$

where the dashed line represents an $f^+(\mathbf{r})$ function, i.e., the probability for overlap in the case of permeable objects. Hence $f^+(\mathbf{r}) = 1$ within the region of possible overlap (the excluded volume^{7,18}) and $f^+(\mathbf{r}) = 0$ outside this region. For permeable objects one can also define^{3,6,7} $f^* = -f^+$ such that

$$\text{O} \cdots \text{O} = \int f^*(\mathbf{r}) d^3r .$$

The new extension is that we have here ‘‘different objects’’ so that we may assign to every point in the diagram a certain type of object (e.g., a different ‘‘type’’ of box). We thus have two types of contributions to c_2^+ : from boxes which have their L edges parallel to each other, and from boxes which have their L edges perpendicu-

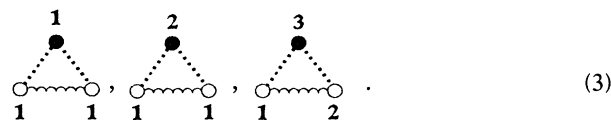
lar to each other. These can be represented by two types of diagrams, i.e.,



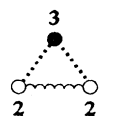
denoting an overlap of two type-1 boxes, and



denoting an overlap of a type-1 and a type-2 box. For c_3^+ we have three types of relevant diagrams:



All other diagrams, such as



are obtained from these by changing the names of the axes (thereby leaving the numerical value of the corresponding integrals unchanged) but they may appear with different statistical weights due to a possible anisotropy in the distribution of the boxes along the axes. As shown below c_4^+ has already many more types of diagrams. The quickly rising number of possible types of objects' overlaps along with the increasing number of diagrams makes the calculation of higher terms increasingly tedious and difficult.

In summing the contributions for $c^+(0)$ it is easy to see that each diagram must be weighted by the probability of its points (i.e., of the objects assigned to the point) being of a given type. Correspondingly we introduce the numbers m_1, m_2, m_3 , the number of type-1, -2, and -3 boxes, respectively. We further define $m = m_1 + m_2 + m_3$ and $x_i = m_i/m$. We have usually normalized the m_i 's so that the smallest value of m_i is equal to 1. Thus $m_1 = 50, m_2 = m_3 = 1$, means that there are 50 type-1 boxes to every type-2 and -3 box. Considering all types of boxes, we have

$$c_2^+ = \sum x_i^2 \text{O} \cdots \text{O} + \sum x_i x_j \text{O} \cdots \text{O} , \tag{4}$$

where the first summation is over $i = 1, 2, 3$, while the second summation is over $i, j = 1, 2, 3$, but $i \neq j$. Similarly for c_3^+ we obtain

$$c_3^+ = \sum x_i^3 \text{O} \cdots \text{O} + 2 \sum x_i^2 (x_j + x_k) \text{O} \cdots \text{O} + 6 \prod x_i \text{O} \cdots \text{O} , \tag{5}$$

where the summations and product are over $i = 1, 2, 3$ in all the terms and j, k are chosen so that (i, j, k) is a cyclic permutation of $(1, 2, 3)$. For c_4^+ , the situation is more complex and while in the simple ‘‘single object type’’

case^{6,7} one has that

$$c_4^+ = \frac{3}{2} \left[\text{Diagram 1} \right] + \frac{7}{2} \left[\text{Diagram 2} \right] + \left[\text{Diagram 3} \right],$$

in the present case, after having assigned all possible types of boxes to all points and having contracted somewhat the results, we get that

$$c_4^+ = \frac{3}{2} \left[\sum x_i^4 \left(\text{Diagram 1} \right) + 4 \sum x_i^3 (x_j + x_k) \left(\text{Diagram 2} \right) + \sum x_i^2 (x_j^2 + x_k^2) \left(\text{Diagram 3} + \text{Diagram 4} \right) + 2 \sum x_i^2 x_j x_k \left(\text{Diagram 5} + \text{Diagram 6} \right) \right] + \frac{7}{2} \left[\sum x_i^4 \left(\text{Diagram 7} \right) + \sum x_i^3 (1 - x_i) \left(\text{Diagram 8} + \text{Diagram 9} \right) + \sum x_i^2 (x_j^2 + x_k^2) \left(\text{Diagram 10} + \text{Diagram 11} \right) + 2 \sum x_i^2 x_j x_k \left(\text{Diagram 12} + \text{Diagram 13} + \text{Diagram 14} \right) \right] + \left[\sum x_i^4 \left(\text{Diagram 15} \right) + 4 \sum x_i^3 (1 - x_i) \left(\text{Diagram 16} \right) + 3 \sum x_i^2 (x_j^2 + x_k^2) \left(\text{Diagram 17} \right) + 12 \sum x_i^2 x_j x_k \left(\text{Diagram 18} \right) \right], \tag{6}$$

where the summations are over $i, j, k = 1, 2, 3$; j and k are chosen so that (i, j, k) is a cyclic permutation of $(1, 2, 3)$.

Once we have the diagrammatic representations (4), (5), and (6) we can proceed to the numerical evaluations of the c_i^+ 's by calculating the corresponding integrals. For example, the trivial c_2^+ integrals are of two types:

$$\int f_{11}^+(\mathbf{x}) d^3x = 8Ld^2 \equiv (V_{\text{exc}})_{11} \tag{7}$$

and

$$\int f_{12}^+(\mathbf{x}) d^3x = 2d(L+d)^2 \equiv (V_{\text{exc}})_{12}, \tag{8}$$

where $\mathbf{x} = \mathbf{r}_1 - \mathbf{r}_2$, $f_{11}^+(\mathbf{x})$ is the probability of overlap for two boxes, the long edges of which are parallel to the 1 axis, and $f_{12}^+(\mathbf{x})$ is the probability of overlap for two boxes for which the long edges are perpendicular. The volumes so determined are the well-known excluded volumes¹⁸ of these configurations. In general, $f_{ij}^+(\mathbf{x})$ is the probability of overlap for two boxes, when the elongated edge of one lies in the i direction, and the elongated edge of the other lies in the j direction.

The integrals in c_3^+ and c_4^+ are not as easily evaluated as those in c_2^+ . We therefore present here the method we used to calculate them: We shall demonstrate it on the integral

$$I = \int f_{12}^+(\mathbf{x}) f_{11}^+(\mathbf{y}) f_{12}^+(\mathbf{x}-\mathbf{y}) d\mathbf{x} d\mathbf{y}.$$

As shown in Fig. 1(a), $f_{12}^+(\mathbf{x})$ has a value of unity inside an $(L+d) \times (L+d) \times 2d$ box, whose short edge lies parallel to the 3 direction; $f_{11}(\mathbf{x})$, as shown in Fig. 1(b), has a value of unity within a box of dimensions $2L \times 2d \times 2d$, whose long edge lies along the 1 axis. We can consider the contributions to the integral independently for each axis. This is the essential simplification offered by the use of boxes. We consider the 1 axis first. Figure 1(c) is a projection of the situation represented by the product $f_{12}^+(\mathbf{x}) f_{12}^+(\mathbf{x}-\mathbf{y})$ for a given \mathbf{y} in the 1-2 plane. The integral of this product over x_1 (the first component of the vector \mathbf{x}) is simply the length of the overlap of the functions $f_{12}^+(\mathbf{x})$ and $f_{12}^+(\mathbf{x}-\mathbf{y})$ considered as functions of \mathbf{x} only. Direct inspection easily shows that this length is equal to $L+d-|y_1|$, if $|y_1| \leq L+d$, and zero otherwise (y_1 is the first component of the vector \mathbf{y}). The presence of $f_{11}(\mathbf{y})$ limits the overlap length, however, to y_1 's such that $|y_1| \leq L$. The 1-axis contribution to the integral is therefore $2 \int_0^L (L+d-y_1) dy_1 = L^2 + 2Ld$.

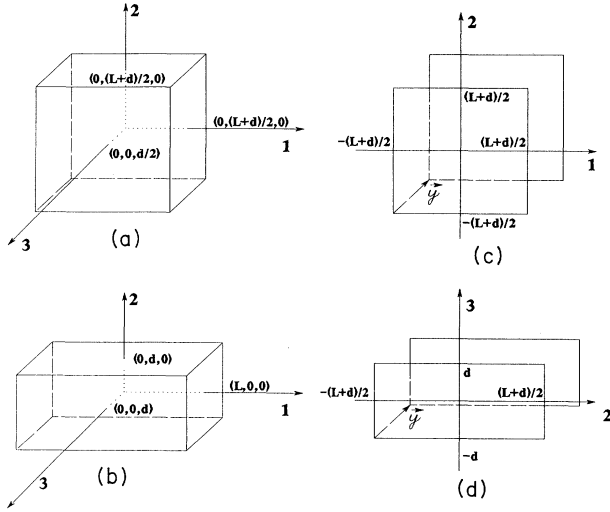


FIG. 1. The geometries associated with the present calculations. (a) The excluded volume between a type-1 box and a type-2 box. Along the 1 axis, the type-2 box's center cannot come closer than $d/2$ to the surface of the type-1 box, which lies a distance $L/2$ from the origin. Hence the excluded volume edge along the axis is $(L+d)/2$. Similar reasoning applies to other axes as well. (b) The excluded volume of boxes in parallel (here both type-1 boxes). This volume is similar in shape to the box itself, but all dimensions are twice as large. Hence the long side is $2L$ and the short side is $2d$. (c) A projection of the product $f_{12}^+(\mathbf{x})f_{12}^+(\mathbf{x}+\mathbf{y})$ onto the 1-2 plane. The functions are 1 within the squares and 0 outside. (d) A projection of the product $f_{12}^+(\mathbf{x})f_{12}^+(\mathbf{x}+\mathbf{y})$ onto the 2-3 plane. As before, the functions are 1 within the shapes and 0 outside.

Identical reasoning applies to the 2 axis, the only difference being the limitation of y_2 to a narrower range of values, i.e., $|y_2| \leq d$, because of the presence of $f_{11}(\mathbf{y})$. As a result, the 3-axis contribution is only

$$\begin{aligned} (V_{\text{exc}}/d^3)k_4 = & \tilde{C} \frac{1732}{27} \eta^3 + (\tilde{B} - \tilde{C}) \left(\frac{98}{3} \eta^4 + \frac{4952}{27} \eta^3 + \frac{166}{3} \eta^2 - \frac{196}{9} \eta + \frac{188}{27} \right) + (2\tilde{D}) \left(\frac{79}{3} \eta^5 + \frac{1165}{9} \eta^4 - \frac{4186}{27} \eta^3 + \frac{475}{3} \eta^2 + \frac{589}{3} \eta + \frac{796}{27} \right) \\ & + (\tilde{A}^2 - \tilde{C}) \left(\frac{100}{27} \eta^6 + \frac{211}{18} \eta^5 + \frac{1381}{18} \eta^4 + \frac{1067}{9} \eta^3 - \frac{17}{9} \eta^2 - \frac{59}{6} \eta - \frac{353}{54} \right), \end{aligned} \quad (12)$$

with

$$\tilde{A} \equiv \sum_{i=1}^3 x_i^2, \quad \tilde{B} \equiv \sum_{i=1}^3 x_i^3, \quad \tilde{C} \equiv \sum_{i=1}^3 x_i^4, \quad \tilde{D} \equiv x_1 x_2 x_3.$$

Returning now to the mean cluster size we can write Eq. (1) in the form^{6,7}

$$S = \left[1 - \sum_{l=2}^{\infty} k_l(B)^{l-1} \right]^{-1} = \sum_{i=0}^{\infty} s_i(B)^i, \quad (13)$$

where $B = \rho \langle V_{\text{exc}} \rangle$, $s_0 = 1$, $s_1 = 1$, $s_2 = 1 + k_3$, and $s_3 = k_4 + 2k_3 + 1$.

As pointed out above, since we know so far only the

$2 \int_0^d (L+d-y_2) dy_2 = 2Ld + d^2$. Figure 1(d) is a projection of the product $f_{12}^+(\mathbf{x})f_{12}^+(\mathbf{x}-\mathbf{y})$ onto the 2-3 plane for a given \mathbf{y} . Direct inspection shows the overlap of $f_{12}^+(\mathbf{x})$ and $f_{12}^+(\mathbf{x}-\mathbf{y})$ along the 3 axis to be $2d - |y_3|$ if $|y_3| \leq 2d$ and zero otherwise. However, $f_{11}^+(\mathbf{y})$ imposes a further limit $|y_3| \leq d$, thereby reducing the 3-axis contribution to $2 \int_0^d (2d - y_3) dy_3 = 3d^2$.

The full integral is therefore the product of all the contributions, i.e., it is $I = 3d^2(L^2 + 2Ld)(2Ld + d^2)$. Defining the aspect ratio $\eta = L/d$, we have that $I = d^6 [3(\eta^2 + 2\eta)(2\eta + 1)]$. We have similarly calculated all the diagrams that appear in c_3^+ and c_4^+ . The results are collected in Table I.

Once c_3^+ and c_4^+ are calculated, we obtain ρ_c to this order using the $\rho_c = 1/c^+(0)$ divergence condition [Eq. (1)]. A more useful quantity, however, is the dimensionless number B_c (average bonds per object), defined commonly¹⁸ as $B_c = \rho_c V_{\text{exc}}$ where V_{exc} is the excluded volume of two potentially overlapping objects. Since, in our system of boxes, there are several excluded volumes, we define the critical average number of bonds per site,¹⁸ $B_c = \rho_c \langle V_{\text{exc}} \rangle$, by the expectation value of the above excluded volumes, i.e.,

$$\langle V_{\text{exc}} \rangle = \sum_{i,j=1,2,3} x_i x_j \langle V_{\text{exc}} \rangle_{ij} = c_2^+, \quad (9)$$

where $i, j = 1, 2, 3$. Using Eqs. (7)–(9) and the fact that $\sum_{i=1}^3 x_i = 1$ we have that

$$\langle V_{\text{exc}} \rangle = 2d^3 \left[(1 + \eta)^2 - \sum_{i=1}^3 x_i^2 (1 - \eta)^2 \right]. \quad (10)$$

Similarly by defining^{6,7} $k_l = c_l^+ / \langle V_{\text{exc}} \rangle^{l-1}$, we obtain from Eq. (5) and the results given in Table I that

$$\begin{aligned} (V_{\text{exc}}/d^3)^2 k_3 = & -27\tilde{B}\eta^2 - 9(\tilde{A} - \tilde{B})(2\eta^3 + 5\eta^2 + 2\eta) \\ & - 6\tilde{D}(1 + 2\eta)^3 \end{aligned} \quad (11)$$

and from Eq. (6) and Table I that

coefficients k_2 , k_3 , and k_4 we have used a biased Padé approximants method¹⁹ to obtain better quantitative results for B_c . The procedure used to derive these approximants was exactly the one we have previously described,⁷ i.e., we introduce the function $[S(B)]^{1/\gamma} \equiv F(B)$, where γ is the cluster critical exponent, which we assume to be universal and thus given. The power-series expansion of F is then²⁰

$$F(B) = \sum_{i=0}^{\infty} f_i(B)^i, \quad (14)$$

with $f_0 = 1$, $f_1 = ns_1$, $f_2 = \frac{1}{2}(n-1)s_1 f_1 + ns_2$, and $f_3 = f_1 s_2 (n-1) + \frac{1}{6} f_1 s_1^2 (n-1)(n-2) + ns_3$, where

TABLE I. The diagram values.

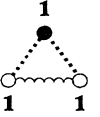
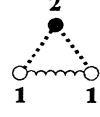
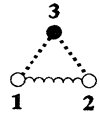
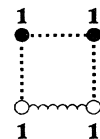
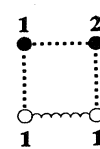
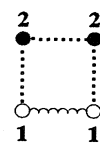
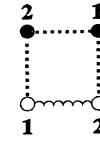
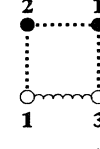
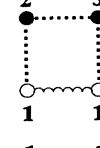
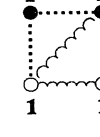

| | | |
|---|--|-------------------|
|  | $=d^6(27\eta^2)$ | $\text{sgn} = -1$ |
|  | $=d^6[3(\eta^2 + 2\eta)(2\eta + 1)]$ | $\text{sgn} = -1$ |
|  | $=d^6(1 + 2\eta)^3$ | $\text{sgn} = -1$ |
|  | $=d^9(16\eta/3)^3$ | $\text{sgn} = -1$ |
|  | $=d^9[\frac{16}{9}(1 + \eta)^2(5\eta - 1)(\frac{4}{3} + 4\eta)]$ | $\text{sgn} = -1$ |
|  | $=d^9[\frac{16}{3}(2\eta^2 + 4\eta - \frac{2}{3})^2]$ | $\text{sgn} = -1$ |
|  | $=d^9[(\frac{4}{3})^3(1 + \eta)^6]$ | $\text{sgn} = -1$ |
|  | $=d^9[32(\eta^2 + 2\eta - \frac{1}{3})(\eta + \frac{1}{3})^2]$ | $\text{sgn} = -1$ |
|  | $=d^9[\frac{32}{3}(1 + \eta)^3(\frac{1}{3} + \eta)^2]$ | $\text{sgn} = -1$ |
|  | $=d^9[14\eta/3]^3$ | $\text{sgn} = +1$ |
|  | $=d^9[\frac{14}{3}(4\eta + \frac{2}{3})(\eta^3 + 3\eta^2 + \eta - \frac{1}{3})]$ | $\text{sgn} = +1$ |

TABLE I. (Continued).

| | | |
|--|--|-----------|
| | $=d^9[\frac{14}{3}(\frac{5}{3}+3\eta)(5\eta^3/3+3\eta^2)]$ | sgn = + 1 |
| | $=d^9[\frac{14}{3}(2\eta^2+3\eta-\frac{1}{3})^2]$ | sgn = + 1 |
| | $=d^9\{\frac{56}{27}[(1+\eta)^3-1]\}^2$ | sgn = + 1 |
| | $=d^9(\frac{5}{3}+\eta+2\eta^2)(\frac{5}{3}+3\eta)(\frac{2}{3}+4\eta)$ | sgn = + 1 |
| | $=d^9\frac{2}{3}[(1+\eta)^3-1](3\eta+\frac{5}{3})^2$ | sgn = + 1 |
| | $=d^9\frac{2}{3}[(1+\eta)^3-1](4\eta+\frac{2}{3})^2$ | sgn = + 1 |
| | $=d^9(4\eta)^3$ | sgn = - 1 |
| | $=d^9[4(1+3\eta)(3\eta^2+\eta^3)]$ | sgn = - 1 |
| | $=d^9\{[2(\eta+1)(3\eta+1)][\frac{7}{12}(1+\eta)^3-\frac{2}{3}]\}$ | sgn = - 1 |
| | $=d^9[2(\eta+\eta^2)(1+3\eta)^2]$ | sgn = - 1 |

$n \equiv 1/\gamma$. Assuming that, as $B \rightarrow B_c$ we have that $S(\rho) \sim A/(\rho - \rho_c)^\gamma$, we obtain that

$$[S(\rho)]^{1/\gamma} \equiv F \sim 1/(\rho - \rho_c). \tag{15}$$

A finite sum for F , however, such as we have here, does not diverge anywhere. One therefore assumes a divergent functional form for $F(B)$, the simplest of which is a rational function $P(L, M)$, the well-known Padé approximant. We have¹⁹ then that

$$P(L, M) = \left[1 + \sum_{j=1}^L a_j B^j \right] / \left[\sum_{j=0}^M b_j B^j \right], \tag{16}$$

where the coefficients a_j and b_j are determined by equating $F(B)$ of Eq. (14) with this expression of $P(L, M)$. Clearly, $L + M$ is determined by the highest known order in the S or F series (in our case $L + M = 3$). Past experience^{7,8} shows that the diagonal (or "middle") term (here $M = 2$) gives the best quantitative result. Once the b_j 's are determined, we can look for B_c by finding the poles of P (which are expected due to the asymptotic divergence of F [see Eq. (15)]. Hence we simply calculated $B_c(1, 2)$ by solving the denominator of $P(1, 2)$. It is easily seen that the corresponding B_c i.e., $B_c(1, 2) \equiv [-B_1 - (B_1^2 - 4B_2)^{1/2}]/(2B_2)$ where $B_1 \equiv (f_1 f_2 - f_3)/(f_2 - f_1^2)$ and $B_2 \equiv -f_2 - f_1 B_1$.

III. RESULTS

We have calculated B_c for a variety of aspect ratios, η , and several macroscopic anisotropies (m_1, m_2, m_3). Our results, which are shown in the following figures, are presented by the dependence of $B_c(1, 2)$ on η and m_1/m_2 . Figure 2 contains the results of our calculations of $B_c(1, 2)$

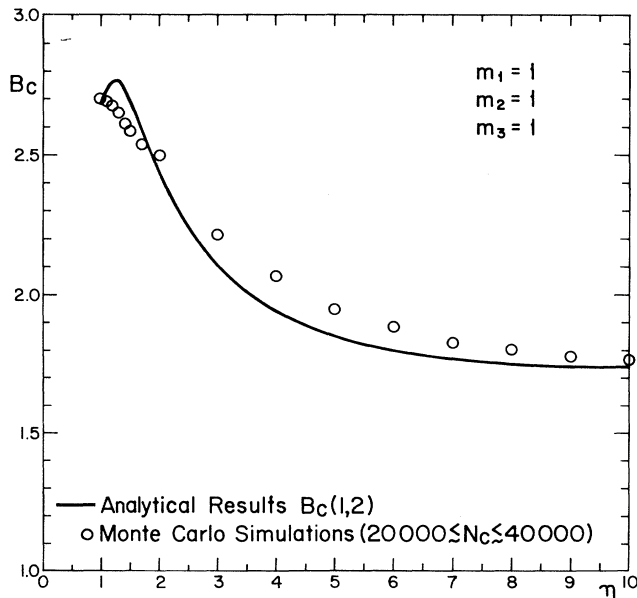


FIG. 2. The dependence of the percolation threshold on the aspect ratio for a macroscopically isotropic ($m_1 = m_2 = m_3 = 1$) system of elongated boxes.

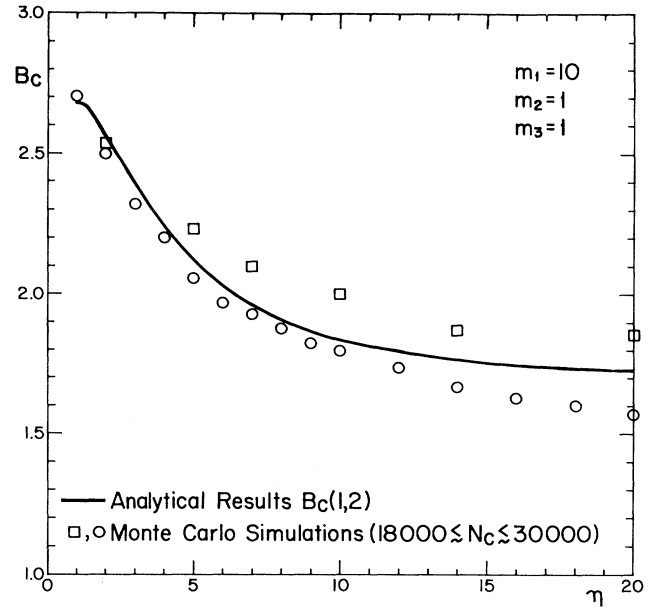


FIG. 3. The dependence of the percolation threshold on the aspect ratio for a system of elongated boxes. The macroscopic anisotropy of the system is $m_1/m_2 = 10$.

for the isotropic distribution ($m_1 = m_2 = m_3 = 1$), for a range of aspect ratios. For comparison, we also present the results of our Monte Carlo simulations. As one sees, the quantitative agreement between the two results is striking. Our calculations fit the Monte Carlo simula-

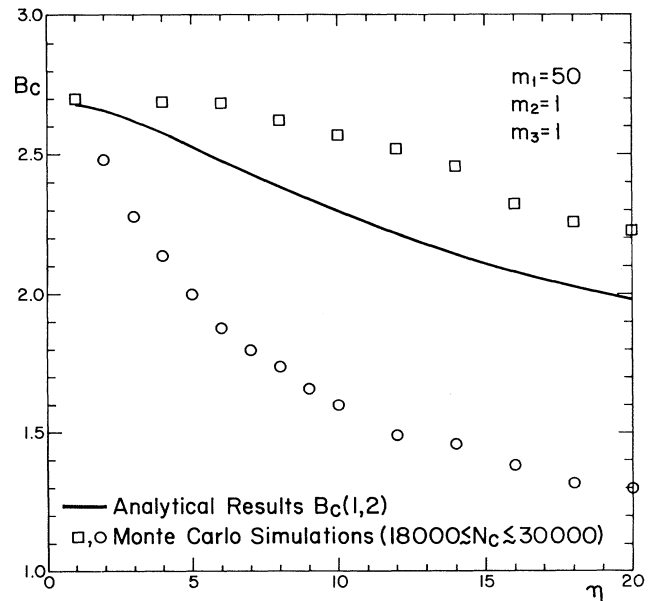


FIG. 4. The dependence of the percolation threshold on the aspect ratio for a system of elongated boxes. The macroscopic anisotropy of the system is $m_1/m_2 = 50$.

tions to within 5%. Around $\eta=2$, the Monte Carlo simulations show an inflection point, where the graph changes from convex to concave behavior. This effect is reproduced by our calculations, but most likely the Padé approximant method enhances it exaggeratedly. This is most probably the origin of the artificial local maximum at $\eta \approx 1.2$. Still, even in this range, the discrepancies between our results and the Monte Carlo simulations are less than 5%. Similar effects appear in other macroscopic anisotropies, but the local maximum rapidly diminishes until by $m_1/m_2=50$ it is entirely unnoticeable. The fact that usually the Monte Carlo results are systematically somewhat higher than our calculated results may well be attributed to finite-size effects in the simulations.

We have considered next the effects of macroscopic anisotropy (that is, $m_1 \neq m_2$) on the percolation threshold. The $B_c(1,2)$ dependence on the aspect ratio η for the case $m_1/m_2=10$ is shown in Fig. 3, while the $m_1/m_2=50$ case is shown in Fig. 4. The two cases are shown since comparison with Monte Carlo results for an anisotropic system is somewhat delicate. It is well known^{21,22} that finite macroscopically anisotropic systems of elongated objects display two different percolation thresholds. When determined along the direction parallel to the long edge of most boxes, the threshold is systematically lower than if determined along the direction perpendicular to it. The convergence of the two sets of data points to the same (infinite sample) value of the percolation threshold, with increasing sample size, is well known to exist for such anisotropic systems.^{21,22} Consequently, we have compared our analytic results with the two Monte Carlo thresholds. Our calculations are seen to be embraced by the two sets of data points. For $m_1/m_2=10$, the two Monte Carlo values are quite close, and our calculations fit them very well. For large anisotropies ($m_1/m_2=50$) there is a large spread in the results but, again, our results fall between them, where one expects the actual (infinite

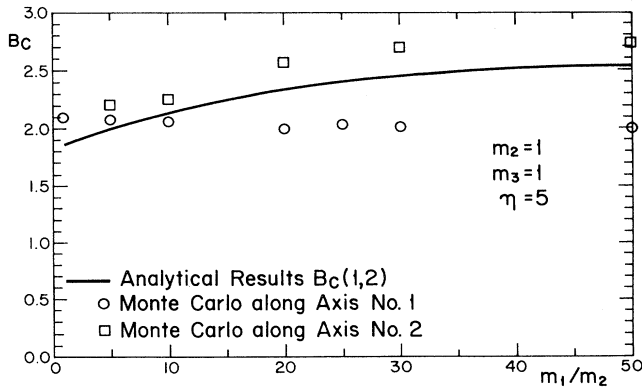


FIG. 5. The dependence of the percolation threshold on the macroscopic anisotropy of the system for a system of elongated boxes with an aspect ratio of $\eta=5$.

sample) value to be. This value may be evaluated by some type of averaging of the two sets of data points. Since, however, our primary interest here is the analytic calculation, we shall deal with the simulation issues elsewhere.²³

In Fig. 5 we show the dependence of $B_c(1,2)$ on the macroscopic anisotropy for a given aspect ratio. The analytic results are again seen to be embraced by the two sets of Monte Carlo results. Hence the results exhibited by Fig. 5 are another demonstration of the excellent quantitative agreement between the present analytical results and the Monte Carlo simulations. As was remarked before, the small existing deviations between the results of analytic calculation and the results of the simulations reflect the limits of the simulations rather than the limits of the convergence of the order-by-order expansion.²³

IV. DISCUSSION

Prior to the present work there have been several attempts^{5,12,24} to actually calculate percolation thresholds by analytical methods. All were centered around choosing an approximate functional form for $c^+(\mathbf{r})$, usually in terms of the two particle correlation function of some corresponding system. The most widely used among such functional forms (also known as a closure) is undoubtedly the Percus-Yevick (PY) approximation. However, this closure is easily applicable only in the case of three-dimensional spheres. Even then, quantitative results are quite poor. Using the PY approximation, one gets⁵ $B_c=4.0$ for the aforementioned system, instead of the actual $B_c=2.8$ obtained in Monte Carlo simulations. Up to quite recently, there was no attempt to apply Coniglio's theory to systems of anisotropic objects. Some time ago, Sevick, Monson, and Ottino¹¹ used thermodynamic perturbation theory to investigate a system of permeable ellipsoids. Basically, these authors used a system of spherical particles as a "reference system." Object anisotropy was introduced then as a perturbation. The pair connectedness is obtained by corrections of the PY pair-connectedness function of the reference system. In that paper, the authors have limited themselves to a zeroth-order approximation; by their own admission this crude calculation yields basically qualitative results. The numerical difficulties are even at this stage quite formidable, so that no aspect ratio greater than 5 was considered. Since the PY approximation is the starting point of that calculation, it is not surprising that for very small aspect ratios (very slight anisotropies), one recovers the PY results (about 40% higher than Monte Carlo simulations). As the aspect ratio increases, ρ_c decreases, thus improving the adequacy of the PY approximation, so that for $\eta=5$, their results are about 8% higher than the simulations (which may themselves be a little too high due to finite-size effects). As noted before, the mathematics involved prevents practical calculations for anisotropies higher than $\eta=5$. Our method, on the other hand, is *quantitatively* adequate over a wide range of aspect ratios. Since it is analytic, one need not recalculate everything anew for each aspect ratio. It appears therefore to be at

once more flexible and more powerful than the approximation used by Sevick, Monson, and Ottino.

In a recent article,¹² Laria and Vericat have applied reference-interaction-site-model (RISM) method to a system of elongated objects distributed randomly in space. Their objects consist of eight partly overlapping spheres ordered linearly. Thus the maximum aspect ratio considered in their work is $\eta=8$. These objects are distributed with random orientations in space, and are said to be connected if they overlap (that is, they are “permeable molecules”).

The closure of the Ornstein-Zernike relation used in RISM is of the Percus-Yevick type, and produces results of about the same numerical quality. In particular, the permeable sphere limit obtained by both methods is the same, that is, $B_c=4.0$ instead of the correct 2.8 value (see above). As pointed out by the authors themselves, the results of the RISM are essentially qualitative. The one quantitative success they claim is the reproduction of Monte Carlo results obtained by Balberg, Binenbaum, and Wagner.¹⁵ However, such a claim is hard to verify due to the presentation of their results on a log-log scale; these deviate slightly from the Monte Carlo results, but on such a scale, even these small deviations may translate into quite large numerical discrepancies. One cannot therefore judge the *quantitative* adequacy of the results, in the absence of the numbers themselves (although, as noted, qualitative behavior is well reproduced).

The authors of Ref. 12, however, further claim that they obtain the correct critical exponent γ to within 10%, that is 2 instead of 1.8. (More recent results give

$\gamma=1.74$, which is the value we have used in this paper. $\gamma=1.8$ would have produced results very slightly higher than the ones we obtained.) Yet, this is to some extent an artifact of the method used. The RISM closure, like the Percus-Yevick closure, imposes strong restrictions on the dependence of the mean cluster size S upon the density ρ . In effect, the closure determines a polynomial dependence of $1/S$, thereby forcing γ to be an integral number. The 10% exactness of the results is merely the reflection of the fact that γ itself is so close to being an integer. One might even say that this circumstance is one of the reasons the PY or RISM approximations work fairly well, as there is no true first-principles understanding of their validity.

We do not see therefore any specific advantage in the RISM approach. In contradiction, our results are *quantitatively* sound. As for our use of the value of γ in the biased Padé coefficients, it does not seem to be such a drawback, as RISM (or PY) theory does not really provide added insight into its value. Furthermore, our approach has the advantage that it yields naturally not only the aspect ratio dependence of ρ_c (or B_c) but also its dependence on the system's anisotropy. Such results have not been presented before.

In conclusion, the order-by-order diagrammatic expansion enabled us to obtain the first qualitative as well as *quantitatively accurate* analytic determination of percolation thresholds in continuum systems which are macroscopically anisotropic. Hence the diagrammatic expansion used appears to provide a useful basis for a rigorous nonlattice theory of continuum percolation.

¹D. Stauffer, *Introduction to Percolation Theory* (Taylor and Francis, London, 1985).

²I. Balberg, *Philos. Mag. B* **56**, 991 (1987).

³A. Coniglio, U. De Angelis, and A. Forlani, *J. Phys. A* **10**, 1123 (1977); A. Coniglio, U. De Angelis, and G. Lauro, *ibid.* **10**, 219 (1977).

⁴This function and its applications in fluid theory are discussed in many textbooks of statistical mechanics. See, for example, J. P. Hansen and I. R. M. Macdonald, *Theory of Simple Liquids* (Academic, New York, 1976).

⁵T. De Simone, R. M. Strat, and S. Demoulini, *Phys. Rev. Lett.* **56**, 1140 (1986).

⁶A. L. R. Bug, S. Safran and I. Webman, *Phys. Rev. Lett.* **54**, 1412 (1985); *Phys. Rev. B* **33**, 4716 (1986).

⁷U. Alon, A. Drory, and I. Balberg, *Phys. Rev. A* **42**, 4634 (1990).

⁸See for example, J. W. Essam and M. E. Fisher, *J. Chem. Phys.* **38**, 802 (1962); J. Adler, *J. Phys. A* **18**, 1063 (1983).

⁹*Physics and Chemistry of Porous Media*, edited by D. L. Johnson and P. N. Sen (AIP, New York, 1984). In particular, see the paper by E. D. Pittman (p. 1) concerning the pores geometry. For physical applications see I. Balberg, *Phys. Rev. B* **33**, 3618 (1986); I. Balberg, N. Wagner, D. W. Hearn, and J. A. Ventura, *Phys. Rev. Lett.* **60**, 1887 (1988).

¹⁰B. I. Shklovskii and A. L. Efros, *Electronic Properties of Doped Semiconductors* (Berlin, Springer-Verlag, 1983). In particular, see A. S. Skal and B. I. Shklovskii, *Fiz. Tekh. Poluprovodn.* **7**,

1589 (1974) [*Sov. Phys.—Semicond.* **7**, 1058 (1974)].

¹¹E. M. Sevick, P. A. Monson, and J. M. Ottino, *Phys. Rev. A* **38**, 5376 (1988).

¹²D. Laria and F. Vericat, *Phys. Rev. B* **40**, 353 (1989).

¹³W. G. Hoover and A. G. DeRocco, *J. Chem. Phys.* **36**, 3141 (1962).

¹⁴See for example, W. Xia and M. F. Thorpe, *Phys. Rev. A* **38**, 2650 (1988); I. Balberg, *Phys. Rev. B* **31**, 4053 (1985).

¹⁵I. Balberg, N. Binenbaum, and N. Wagner, *Phys. Rev. Lett.* **52**, 1465 (1984).

¹⁶N. Wagner and I. Balberg, *J. Stat. Phys.* **49**, 369 (1987); N. Wagner, D. Klein, and I. Balberg (unpublished).

¹⁷J. Hoshen and R. Kopelman, *Phys. Rev. B* **14**, 3438 (1976). Our continuum version is very similar to that of E. T. Gawlinski and H. E. Stanley, *J. Phys. A* **14**, 1291 (1981).

¹⁸I. Balberg, C. H. Anderson, S. Alexander, N. Wagner, *Phys. Rev. B* **30**, 3933 (1984).

¹⁹G. Baker and P. Graves-Morris, *Padé Approximants* (Addison-Wesley, New York, 1981).

²⁰*Handbook of Mathematical Functions*, edited by M. Abramowitz and I. A. Segun (Dover, New York, 1968), p. 15.

²¹I. Balberg and N. Binenbaum, *Phys. Rev. B* **28**, 3799 (1983).

²²W. J. Boudville and T. C. McGill, *Phys. Rev. B* **39**, 369 (1989).

²³A. Drory, I. Balberg, and B. Berkowitz (unpublished).

²⁴Y. C. Chiew and E. D. Glandt, *J. Phys. A* **16**, 2599 (1983); Y. C. Chiew, G. Stell, and E. D. Glandt, *J. Chem. Phys.* **83**, 761 (1985).